Journal of Materials Chemistry C

ROYAL SOCIETY OF CHEMISTRY

PAPER

View Article Online
View Journal | View Issue

Cite this: J. Mater. Chem. C, 2025, 13, 8470

Flexible organic–inorganic hybrid crystals of tin(IV) chloride and naphthalenediimide: exploring elasticity, mechanochromism, and photothermal conversion†

Sotaro Kusumoto, *[a] Shunya Masuda,[a] Ryo Suzuki, [b] Masaru Tachibana, [b] Masaya Shimabukuro, [c] Mamiko Kobayashi,[c] Naoki Ogiwara, [d] Sayaka Uchida, [d] Tomoya Fukui,[e] Yuta Tsuji, [f] Masaya Okamura, [a] Shiro Hikichi, [a] Yang Kim[g] and Yoshihiro Koide*[a]

Received 28th February 2025,
Accepted 19th March 2025

DOI: 10.1039/d5tc00891c

rsc.li/materials-c

Organic–inorganic hybrid metal halides (OIMHs) are emerging functional materials with diverse applications. However, the exploration of mechanically soft OIMHs remains limited. This study introduces tin(IV) OIMH crystals (**1** and **1w**), incorporating a naphthalenediimide (NDI)-based organic cation (**3pmNDI**), which exhibit elastic flexibility, mechanochromism, and photothermal conversion. The unique one-dimensional (1D) slip-stacked assembly of **3pmNDI** cations, influenced by the presence or absence of lattice water (**1w** *vs.* **1**), dictates their mechanical properties and chromic behavior. Compound **1** exhibits an exceptionally low elastic modulus (E_r = 1.84 ± 0.21 GPa), as measured by nanoindentation, and a photothermal conversion efficiency of 63%. These findings showcase the potential of OIMHs as multifunctional flexible crystals.

Introduction

Soft crystalline materials have garnered considerable attention recently due to their remarkable ability to maintain high crystallinity while responding to external stimuli such as vapor exposure,[1] friction,[2] and mechanical stress.[3] These stimuli induce molecular assembly changes over short and long distances, resulting in functional alterations within the materials.[4] This adaptability permits the modulation of properties such as color,[5] crystal morphology,[6] luminescence,[7] magnetism,[8] and electrical conductivity,[9] rendering these materials highly promising for applications in sensors,[10] actuators,[11] and flexible devices.[12] The flexible framework formed by weak molecular interactions, such as van der Waals forces,[13] is a critical factor driving these versatile properties.

In recent decades, materials incorporating π-conjugated molecules stabilized by π–π stacking interactions have garnered significant attention and remain a subject of active study.[14] These materials facilitate one-dimensional anisotropic crystal growth and exhibit exceptional elastic and flexible behaviors.[15] Localized X-ray analysis and spectroscopic measurements have demonstrated that these supramolecular interactions function as buffer components, enabling reversible macroscopic bending. This bending is characterized by expansion in the outer regions of the crystal and intermolecular contraction in the inner regions during deformation.[16] The weak interactions governing molecular assembly allow molecules to shift from their thermodynamic equilibrium positions in response to mild stimuli, thus enabling the modulation and switching of properties even within the crystalline structure.[17] While most studies have focused on neutral organic molecules or coordination complexes,[3,6] mainly due to the significance of van der Waals forces, materials like Organic–inorganic hybrid metal halides (OIMHs)[18]—characterized by spatially extended electrostatic interactions—remain underexplored. This research gap may stem from these materials' inherently strong electrostatic interaction energies, typically an order of magnitude greater than van der Waals forces.[19]

[a] Department of Applied Chemistry, Faculty of Chemistry and Biochemistry, Kanagawa University, 3-27-1 Rokkakubashi, Kanagawa-ku, Yokohama 221-8686, Japan. E-mail: kusumoto@kanagawa-u.ac.jp, ykoide01@kanagawa-u.ac.jp
[b] Department of Materials System Science, Yokohama City University, 22-2 Seto, Kanazawa-ku, Yokohama, Kanagawa 236-0027, Japan
[c] Institute of Biomaterials and Bioengineering, Tokyo Medical and Dental University, 2-3-10, Kanda-Surugadai, Chiyoda-ku, Tokyo 101-0062, Japan
[d] Department of Basic Science, School of Arts and Sciences, The University of Tokyo, 3-8-1 Komaba, Meguro, Tokyo 153-0041, Japan
[e] Laboratory for Chemistry and Life Science, Institute of Integrated Research, Institute of Science Tokyo, 4259 Nagatsuta-cho, Midori-ku, Yokohama, Kanagawa 226-8501, Japan
[f] Faculty of Engineering Sciences, Kyushu University, Kasuga, Fukuoka 816-8580, Japan
[g] Department of Chemistry, Graduate School of Science and Technology, Kumamoto University, 2-39-1 Kurokami, Chuo-ku, Kumamoto 860-8555, Japan

† Electronic supplementary information (ESI) available. CCDC 2417348 and 2417349. For ESI and crystallographic data in CIF or other electronic format see DOI: https://doi.org/10.1039/d5tc00891c

Unlike van der Waals forces, electrostatic interactions may not offer a "buffer space" to absorb mechanical stimuli, complicating efforts to achieve the flexibility and responsiveness characteristic of OIMHs.

OIMHs are unique ionic materials composed of organic cations and metal halide anions, attracting significant interest for potential applications in advanced technologies such as solar cells,[20] lasers,[21] light-emitting diodes (LEDs),[22] and nonlinear optical materials.[23] While considerable progress has been made in understanding their remarkable properties and fundamental mechanical characteristics,[24] developing mechanically soft OIMHs remains largely unexplored. Gaining insights into enhancing their flexibility and enabling macroscopic deformation is vital for broadening their range of applications and contributing to advancing stimuli-responsive materials.

Naphthalenediimide (NDI) stands out due to its redox activity,[25] chemical stability,[26] planarity,[27] π-acidity (electron-accepting nature),[28] and n-type semiconducting behavior.[29] Integrating NDI molecules into OIMHs facilitates anisotropic crystal growth and flexibility through π···π stacking, while also enabling these functionalities.[25–29] This approach paves the way for the development of multifunctional flexible crystals that were previously unattainable.

This study aims to develop mechanically flexible OIMHs that incorporate NDI cations. The tin(IV) halide hybrids exhibit significant crystal flexibility due to the 1D arrangement of NDI units within their crystal structure, marking the observation of elastic deformation in OIMHs. Nanoindentation tests indicate that water-free crystals demonstrate one of the lowest elastic moduli among OIMHs. The soft and dense 1D assembly of NDI units also facilitates mechanochromism. Furthermore, the presence of highly stable radicals within the NDI framework induces absorption in the near-infrared (NIR) region, enabling these materials to function as highly efficient and durable photothermal conversion agents.

Results and discussion

Structural characterization for 1 and 1w

Crystallization of the **3pmNDI** (*N*,*N*′-bis(3-pyridylmethyl)naphthalenediimide) with tin(II) chloride in a 12 M HCl, under static conditions, yielded pale-yellow, needle-like crystals (**1w**) exceeding 5 mm in length. Heating the solution for 6 hours prior to crystallization produced reddish-brown crystals (**1**) less than 1 mm in length (Fig. 1). **1w** and **1** are thus classified as kinetic and thermodynamic products, respectively.

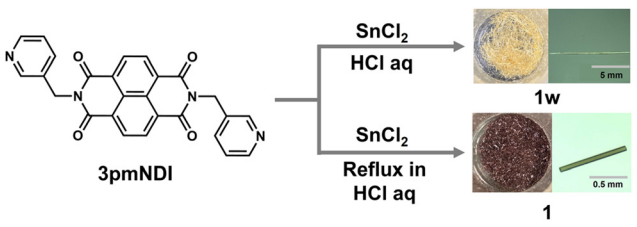

Fig. 1 The synthetic scheme and the appearance of crystals **1** and **1w**.

Single-crystal X-ray diffraction analysis of **1w** and **1** revealed nearly identical structures, differing primarily in the presence of water molecules. **1w** incorporates $[H_2\mathbf{3pmNDI}]^{2+}$ cations, hexacoordinate octahedral $SnCl_6^{2-}$ anions, and 1.5 water molecules, while **1** lacks water molecules (Fig. 2a and c). Both crystallize in the monoclinic $P2_1/c$ space group (Table S1, ESI†) and exhibit 1D π···π stacking interactions along the *a*-axis (Fig. 2). The shortest π···π contacts between NDI units alternate at distances of 3.420 Å and 3.493 Å along the *a*-axis in **1w**, while in **1**, these interactions are consistently measured at 3.350 Å, also aligned along the *a*-axis (Fig. 2b and d). In **1w**, water molecules are interspersed between the 1D π···π stacks, forming hydrogen bonds with adjacent $SnCl_6^{2-}$ and NDI cations (Fig. S1, ESI†). The crystal of **1w** remains intact even when exposed to air, as demonstrated by thermogravimetric analysis (TGA). This analysis reveals a significant decrease in water content around 80 °C (Fig. S2, ESI†). Subsequently, a gradual reduction is observed, with a decrease equivalent to 1.5 water molecules noted near 150 °C. These findings suggest that the water molecules are considerably stabilized at ambient temperature due to hydrogen bonding with neighboring molecules.

Both crystals (**1** and **1w**) obtained under different conditions exhibited good concordance between their PXRD patterns and the simulated patterns derived from the CIF data, demonstrating that these crystals can be selectively synthesized (Fig. S3, ESI†). The NDI moiety is recognized for its exceptional electron-accepting properties;[25,28,29] therefore, the observed color variations between the crystals may be attributed to the presence or absence of free radicals. Electron Spin Resonance (ESR) measurements were conducted to ascertain the presence of organic radicals. A pronounced signal characteristic of organic radicals (g = 2.005) was detected in compound **1**, but not in **1w** (Fig. 3a).

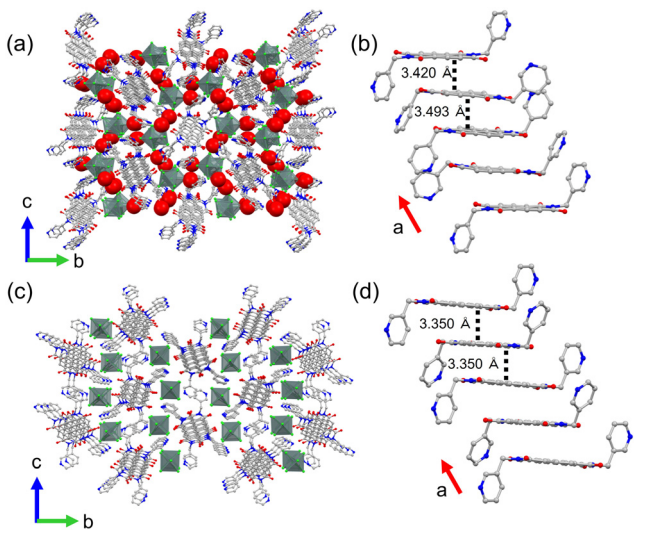

Fig. 2 (a) Packing structure of **1w**, viewed along the *a*-axis. A space-filling model illustrates the arrangement of water molecules. (b) The 1D structure of NDI cations along the *a*-axis of **1w** highlights the nearest NDI-to-NDI distance. (c) The packing structure of **1**, viewed along the *a*-axis. (d) The 1D structure of NDI cations along the *a*-axis of **1** shows the nearest NDI-to-NDI distance.

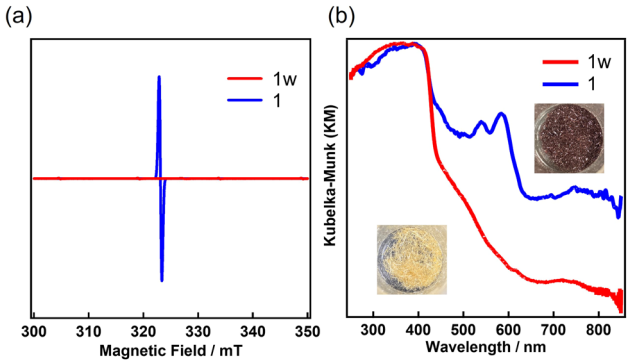

Fig. 3 (a) ESR spectra of **1w** and **1**. (b) Absorption spectra of **1w** and **1**.

The UV-Vis-NIR absorption spectrum of **1** revealed strong charge-transfer bands within the 400–800 nm range (Fig. 3b), consistent with the $NDI^{\bullet -}$ absorptions reported in previously studied NDI-based compounds.[30] Thus, the observed difference in crystal color is attributed to the presence or absence of radicals associated with the NDI moiety.

Density Functional Theory (DFT) calculations on the density of states (DOS) and frontier orbitals were performed to elucidate the electron transfer process. Analysis of the frontier orbitals of compounds **1** and **1w** revealed that the Highest Occupied Molecular Orbital (HOMO) primarily arises from the p-orbitals of chlorine in the $SnCl_6^{2-}$ anions, while the Lowest Unoccupied Molecular Orbital (LUMO) is predominantly composed of the π* orbitals of the NDI moiety (Fig. 4a and b). Fig. 4c and d illustrate that the bands near the Fermi level (set to 0 eV) are mainly attributed to $SnCl_6^{2-}$, whereas the **3pmNDI** cations largely dominate the lowest conduction bands. These theoretical findings suggest that electron transfer from $SnCl_6^{2-}$ to the NDI moiety is likely to occur. When comparing the HOMO–LUMO band gaps, compound **1** exhibits a smaller gap than **1w**. In **1**, the HOMO reveals that the p-orbitals of chlorine in $SnCl_6^{2-}$ interact with neighboring $SnCl_6^{2-}$ units through an antibonding interaction (as indicated by the red arrows in the HOMO of Fig. 4b), which may lead to HOMO destabilization. Conversely, the HOMO of **1w** does not display significant interaction between $SnCl_6^{2-}$ units (Fig. 4a), implying the absence of both stabilization and destabilization. This disparity in interaction may influence the HOMO–LUMO band gap and could be a critical factor facilitating radical generation in **1**.

Remarkably, the radical in **1** exhibits substantial stability, with no observable degradation noted more than a year post-synthesis. This stability is likely attributed to the shielding effect within the crystalline state **1**.[31] The absence of water molecules contributes to a denser structure, which enhances efficient electron transfer and may suppress radical quenching due to reactions with atmospheric oxygen.

Given the 1D aggregation of **3pmNDI** cations, we hypothesized that the radical could function as a charge carrier,[9a,b] impacting electronic conductivity. To investigate this, we conducted conductivity measurements. When a voltage ranging from −2 to 2 V was applied, compound **1** demonstrated a conductivity of 1.8×10^{-9} S cm^{-1}, whereas **1w** exhibited nearly

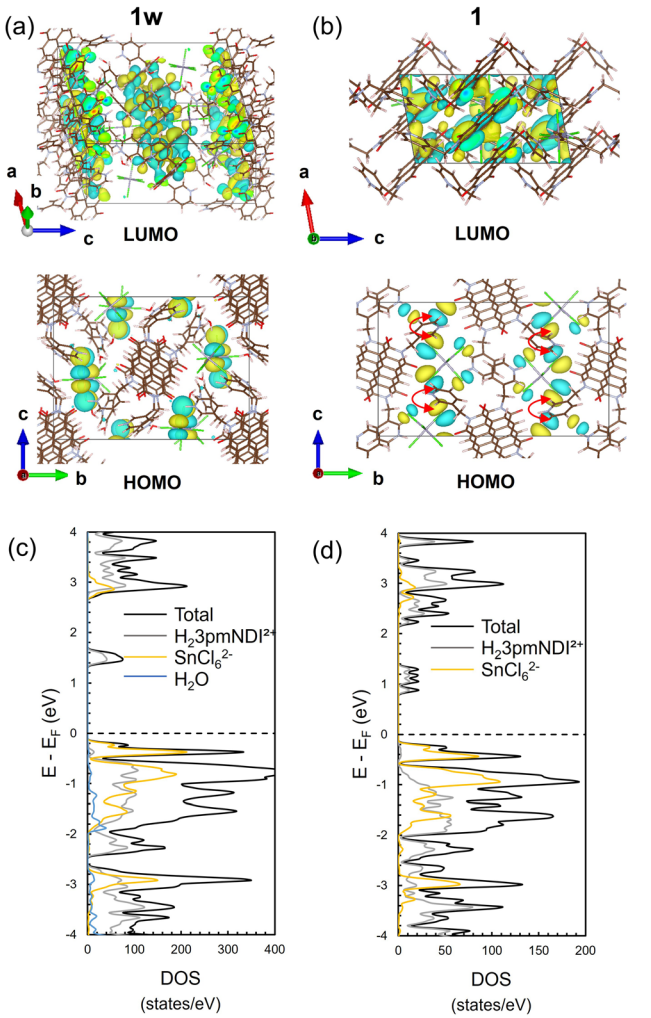

Fig. 4 Calculated frontier orbitals for **1w** (a) and **1** (b). The red arrows in the HOMO of the panel (b) indicate the antibonding orbital interactions. Additionally, panels (c) and (d) display the total and partial density of states calculated from single crystal data for **1w** and **1**, respectively.

insulating behavior with no detectable current flow (Fig. S4, ESI†). Although the conductivity is not exceptionally high, it varies significantly depending on the presence or absence of the organic radical.

Mechanical properties of crystals 1 and 1w

The flexibility of the crystals was confirmed using stress application with a metal needle. Crystals **1w** measured 100–200 μm in thickness and width, with lengths ranging from 5 to 20 mm. Upon applying stress to crystal **1w**, it deformed but returned to its original shape upon removing the stress, demonstrating crystal elasticity (Fig. 5a and Movie S1, ESI†). This finding represents the first documented instance of elastic flexibility in OIMH crystals. Unfortunately, crystals of **1** were too tiny for stress application using a metal needle.

Extensive investigations have been conducted on structure–bending relationships in π-conjugated organic compounds and metal complexes that display elastic bending.[15] These studies

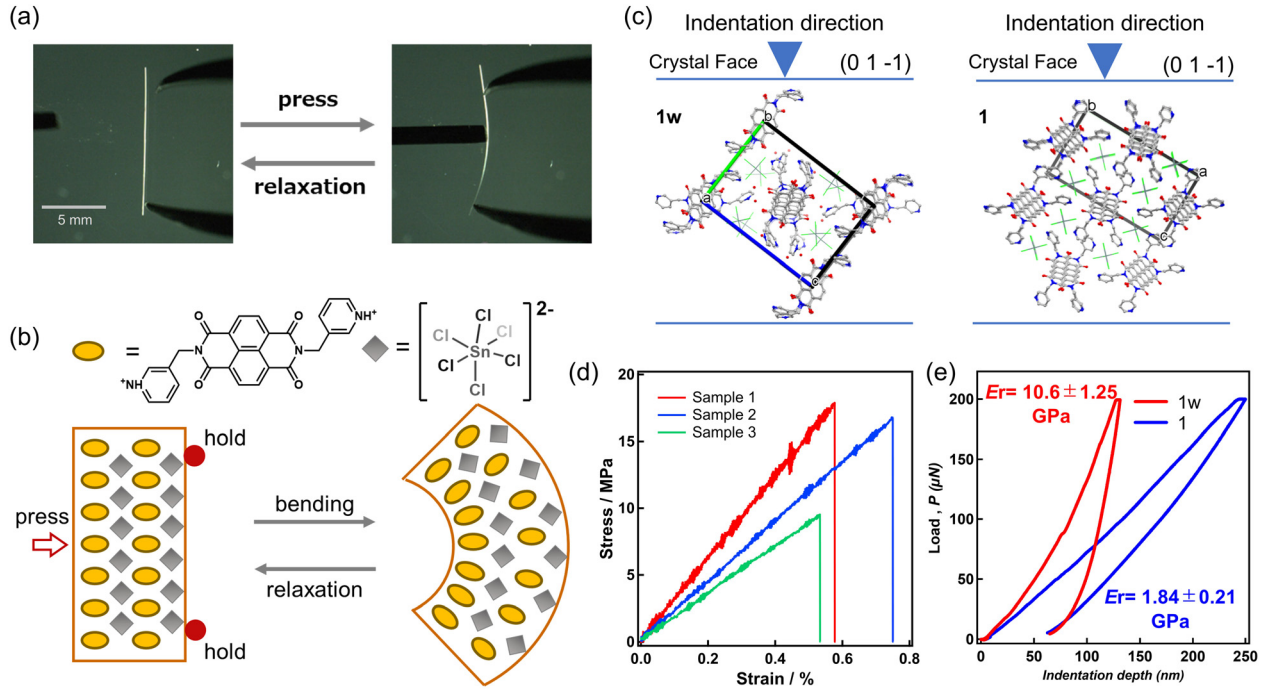

Fig. 5 (a) The elastic deformation of the **1w** crystal. (b) A schematic illustration of elastic deformation. (c) Indentation direction with respect to the crystal structure for mechanical property evaluation. (d) The stress–strain curve from a three-point bending test of the **1w** crystal. (e) The results of the nanoindentation test.

indicate that 1D π···π interactions facilitate flexible elastic deformation, enabling elongation on the outer regions of the crystal and contraction within the inner regions, relative to a thermodynamically stable position (Fig. 5b). Face indexing of crystal **1w** revealed π···π stacking along the *a*-axis, aligning with the primary growth direction of the crystal (Fig. S5, ESI†). Consistent with earlier reports on elastic crystals composed of π-conjugated molecules, these crystals demonstrated growth along the 1D π···π stacking direction, suggesting a similar deformation mechanism.

A three-point bending test was conducted using a universal testing machine to evaluate mechanical flexibility. Crystal **1w** was subjected to stress in the (01−1) direction, and measurements were taken on three samples in total (Fig. 5d and Fig. S6, ESI†). The average elastic modulus obtained was 1.7 GPa, which is relatively low compared to reports on other flexible crystals, indicating significant flexibility (Table S2, ESI†). The maximum elastic strain ranged from 0.53% to 0.76%, which is comparable to that of one-dimensional coordination polymers (0.5–2%) but lower than that of organic crystals (≥2%).[32,33] This can be attributed to the electrostatic interaction between the pyridinium cation and $SnCl_6^{2-}$, which suppresses the intermolecular expansion and contraction of the π···π stacking during deformation. Crystal **1**, however, was too small to be measured using the three-point bending test.

Nanoindentation tests were conducted to determine the hardness (*H*) and reduced modulus (E_r) in the near-surface region of crystals **1w** and **1** (Fig. 5d). The load was applied perpendicular to the 1D π···π stacking of the **3pmNDI** cations in the (01−1) direction (Fig. S5, ESI†). Upon application of 200 μN load to both crystals, the maximum indentation depth was 130 nm for **1w**, while crystal **1** reached a depth of 250 nm, indicating softer mechanical properties in crystal **1**. Due to depth-dependent variations in the reduced modulus (E_r) and hardness (*H*) observed in both crystals (Fig. S7, ESI†), average values were estimated over the range from 150 nm to 250 nm, where the measurements stabilized. For crystal **1w**, the reduced modulus (E_r) and hardness (*H*) were 10.6 ± 1.25 GPa and 0.59 ± 0.07 GPa, respectively, whereas for crystal **1**, these values were significantly lower at 1.84 ± 0.21 GPa and 0.40 ± 0.05 GPa. These results indicate that crystal **1** has a reduced modulus approximately five times lower than **1w** and a hardness reduced by about 0.2 GPa. Specifically, crystal **1** exhibits relatively softer mechanical properties compared to elastic crystals reported in the literature (Table S3, ESI†), reflecting the lowest class of reduced elastic modulus among all reported OIMH crystals (Table 1).[24] The mechanical properties of OIMHs incorporating long alkyl chains have been evaluated by V. P. Dravid *et al.*, revealing extremely low reduced elastic moduli attributable to van der Waals forces between the alkyl chains.[24d] In the compounds investigated in this study, it is suggested that even weak π–π stacking interactions can significantly soften the crystal structure of ionic materials such as OIMHs.

The notable difference in mechanical properties between crystals **1** and **1w** can be attributed to the presence or absence of hydrogen bonding introduced by water molecules (Fig. S1, ESI†). A comparative study was performed using DFT calculations to investigate this intermolecular interaction. From the aggregated structure **1w**, a single $\mathbf{3pmNDI}^{2+}$ molecule was extracted and separated from the remaining part (Fig. S8, ESI†).

Table 1 Mechanical Properties of Selected OIMHs Evaluated Using Nanoindentation

Compounds	E_r (GPa)	H (GPa)	Ref.
$CsPbI_3$	20.1	—	24*b*
$(C1\text{-}NH_3)PbCl_3$ (100)	19.8	0.29	24*c*
PbI_2 (001)	17	0.82	24*b*
$FAPbI_3$ cubic (100)	11.8 ± 1.9	0.37 ± 0.10	24*a*
$FAPbBr_3$ cubic (100)	11.3 ± 0.7	0.43 ± 0.04	24*a*
$(C1\text{-}NH_3)PbI_3$ tetragonal (100)	10.4–14.3	0.42–0.57	24*a*
1w (This study)	**10.6 ± 1.25**	**0.59 ± 0.07**	
[(Me)2-bipy] $[Pb_2I_6]$ (100)	10.5	0.37	24*b*
$(C4\text{-}NH_3)_2PbBr_4$ (out-of-plane)	8.8	—	24*d*
[(Me)2-bipy] $[Pb_2I_6]$ (010)	8.6	0.43	24*b*
$(C4\text{-}NH_3)_2PbBr_4$ (in-plane)	8.1	—	24*d*
$(C4\text{-}NH_3)_2PbI_4$ (in-plane)	5.7		24*d*
$(C4\text{-}NH_3)_2PbI_4$ (out-of-plane)	3.3		24*d*
$(C6\text{-}NH_3)_2PbI_4$ (out-of-plane)	2.1	—	24*d*
$(C8\text{-}NH_3)_2PbI_4$ (out-of-plane)	2.03	—	24*d*
$(C12\text{-}NH_3)_2PbI_4$ (out-of-plane)	2	—	24*d*
1 (This study)	**1.84 ± 0.21**	**0.40 ± 0.05**	
$(C12\text{-}NH_3)_2PbI_4$ (in-plane)	1.3	—	24*d*
$(C6\text{-}NH_3)_2PbI_4$ (in-plane)	0.7	—	24*d*
$(C8\text{-}NH_3)_2PbI_4$ (in-plane)	0.7	—	24*d*

Abbreviation: FA: formamidinium

The energies for these three states were computed, and the intermolecular interaction energy estimated from their differences was found to be 19.6 eV. Following a similar methodology, the intermolecular interaction energy for **1** was calculated to be 18.9 eV, which is 0.7 eV lower than that of **1w**. This decrease in intermolecular interaction energy for **1** corresponds to its reduced mechanical properties compared to crystal **1w**.

Mechanochromic property of 1w

Drawing inspiration from the 1D stacking of NDI and the flexible framework of the crystals, we investigated the mechanochromic behavior of **1w** and **1** through grinding experiments. Initially, a light force was applied to crystal **1w** using a micro spatula, which resulted in no change in its purple luminescence. However, upon applying greater force with a pestle, the luminescence shifted to a yellow-green hue (Movie S2, ESI†). Subsequent exposure to HCl fumes restored the original purple color, indicating that the color change is reversible and demonstrating mechanochromism (Fig. 6a). The emission spectra of the **3pmNDI** itself, **1w**, and the sample after grinding (**1w_grinding**) in the solid state are presented in Fig. 6b. For **3pmNDI**, an emission maximum was observed at 435 nm, accompanied by a shoulder peak at 550 nm. Before grinding, **1w** exhibited an emission maximum at 450 nm and a shoulder at 550 nm, closely resembling the spectrum of **3pmNDI**. This similarity suggests that the emission from **1w** arises from both monomeric and excimer NDI emissions, consistent with previous reports.[34] After grinding, **1w** displayed a broad emission peak with a maximum of 485 nm, which can be attributed to enhanced excimer emission due to the closer proximity of the NDI moieties induced by mechanical stress, aligning with previous reports of mechanochromism driven by excimer emission in NDI compounds.[34]

Single-crystal structural analysis revealed that the π–π interaction distances in **1w** are 3.420 Å and 3.493 Å, which fall within the range of intermolecular distances previously reported for

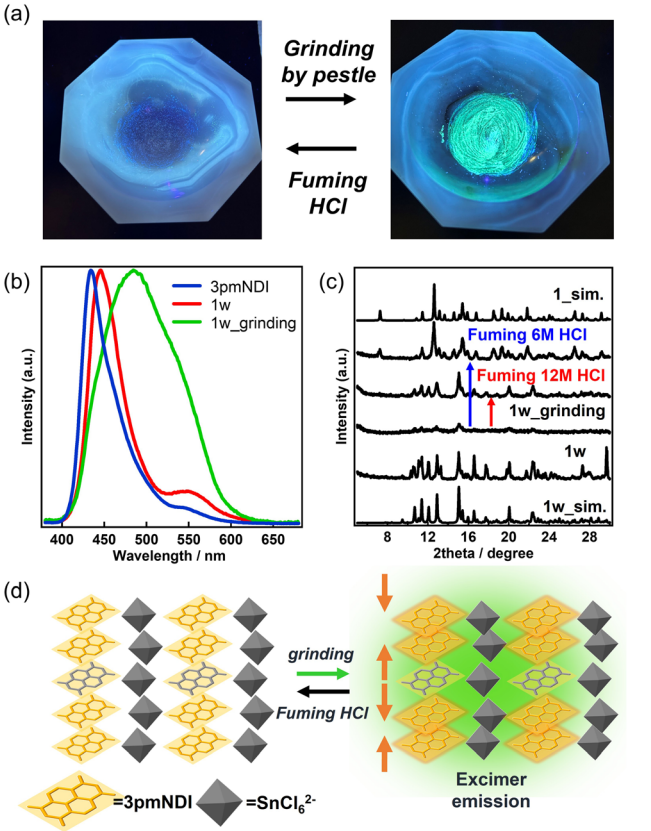

Fig. 6 (a) Mechanochromism observed in **1w**. (b) Emission spectra of **3pmNDI** and **1w** before and after grinding, with λ_{ex}= 350 nm. (c) PXRD patterns of **1w**, showing changes before and after grinding, and exposure to HCl vapor. (d) A schematic illustration depicting mechanochromism caused by excimer emission.

naphthalenediimide derivatives exhibiting excimer emission (Fig. 2b).[34] PXRD analysis demonstrated that **1w**, after grinding with a pestle, exhibited significantly reduced peak intensities, indicating the formation of an amorphous state (Fig. 6c). Following one hour of exposure to 6 M HCl vapor, the **1w_grinding** sample's crystallinity was restored to levels comparable to those of the original **1w**, thereby demonstrating the reversible nature of the chromic phenomenon (Fig. 6c and Fig. S9, ESI†). Furthermore, the vapor diffusion of 12 M HCl into **1w_grinding** for one hour resulted in diffraction peaks distinct from those of **1w**, aligning with the simulated diffraction data for compound **1**. While mechanochromism based on NDI excimer emission has been reported in powdered and liquid crystalline states of organic compounds,[34] this observation represents the first instance in OIMH materials (Fig. 6d). Compound **1** displayed minimal luminescence, which can be attributed to non-radiative transitions induced by the presence of $NDI^{\bullet-}$ (Fig. S10, ESI†). Additionally, no significant changes were observed when powdered **1** was rubbed with a pestle and exposed to UV light (Fig. S10, ESI†).

Photothermal conversion

Materials capable of photothermal conversion, which generate heat from NIR radiation, have attracted significant attention

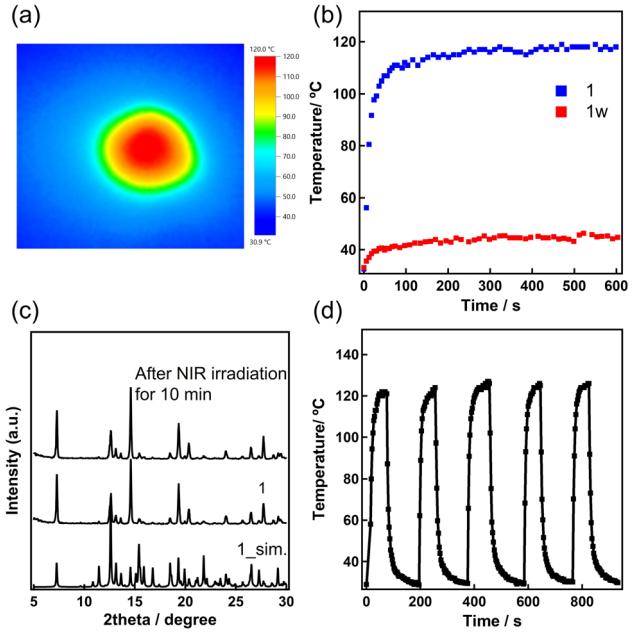

Fig. 7 (a) IR camera images of **1** during NIR light exposure (850 nm, 0.3 W cm^{-2}). (b) Photothermal conversion curves for 10 min. (c) PXRD patterns before and after NIR irradiation. (d) Cyclic photothermal curve upon NIR exposure.

due to their potential applications in various fields, including photothermal therapy (PTT),[35] photothermal/photoacoustic (PT/PA) imaging,[36] and photothermoelectric devices.[37] To demonstrate photothermal conversion capability, a material must absorb light in the appropriate spectral region. After absorption, it transitions from the ground state to an excited state. When it returns to the ground state, it undergoes non-radiative relaxation processes such as internal conversion or intersystem crossing, releasing energy as heat. In the solid state, compound **1** exhibited absorption in the NIR region (Fig. 3b) and demonstrated exceptionally high radical stability, prompting an investigation into its potential as a photothermal conversion material. The photothermal conversion properties of compounds **1** and **1w** under NIR exposure were examined using an IR camera (Fig. 7a). Sample **1w** displayed a minimal temperature increase under NIR laser irradiation (850 nm, 0.3 W cm^{-2}), reaching approximately 45 °C (Fig. 7b). In contrast, **1** exhibited a rapid temperature rise upon NIR laser irradiation, reaching approximately 110 °C within about 100 seconds (Fig. 7b). During the subsequent 10 minutes of irradiation, the temperature remained stable, indicating the high stability of $NDI^{\bullet-}$ at elevated temperatures. The PXRD profile after 10 minutes of NIR irradiation showed almost no change, highlighting the compound's high thermal stability and retention of crystallinity (Fig. 7c). Cyclical experiments (Fig. 7d) confirmed that the material could withstand continuous irradiation for at least five cycles without any degradation in performance, underscoring the durability of $NDI^{\bullet-}$. These findings suggest that compound **1** exhibits excellent photothermal conversion properties, comparable to previous NDI-based materials, with the significant advantage that no additional modifications, such as exposure to amine vapor or UV irradiation, are necessary.[31,38] To our knowledge, this is the first report of photothermal conversion materials based on OIMHs. The cooling and corresponding time–ln(θ) linear curves facilitate calculating photothermal conversion efficiency (Fig. S11, ESI†). The calculated photothermal conversion efficiency (η) was 63%, demonstrating excellent conversion efficiency compared to inorganic materials like Ag_2S (9.5%)[39] and Au nanorods (21%),[40] as well as organic cocrystals (15%),[41] B–N adducts,[42] and MOF materials including Ag–CP (22.1%),[39] perylenediimide MOF (52.3%),[31] and MOFs with viologen ligands (77%).[38]

Conclusions

This study demonstrates that incorporating NDI-based cations into organic–inorganic tin(IV) halide hybrids significantly enhances their crystal flexibility, mechanochromic behavior, and photothermal conversion properties. Nanoindentation measurements revealed that compound **1**, which lacks lattice water, exhibits exceptional flexibility, positioning it among the most flexible OIMHs. Additionally, **1w** displayed mechanochromism attributed to excimer emission between NDI units, supported by its flexible structure. Although excimer emission between NDI units is commonly observed, this study marks the first instance of such behavior in OIMHs. Furthermore, stable NDI radicals generated through electron transfer from $SnCl_6^{2-}$, exhibit NIR absorption, facilitating efficient photothermal conversion. These findings highlight the potential of NDI-based organic–inorganic hybrids to advance the design of soft and multifunctional materials, creating new opportunities for developing flexible and responsive systems.

Experimental

Materials and instruments.

All chemicals and solvents used in the preparation were obtained from Tokyo Kasei Co. and Wako Pure Chemical Industries, Ltd. and were used without further purification. The **3pmNDI** was prepared following the reported method with minor modifications.[43]

Syntheses of 3pmNDI and OIMHs (1 and 1w)

Synthesis of *N*,*N*'-bis(3-pyridylmethyl)naphthalenediimide (3pmNDI). Naphthalene-1,4,5,8-tetracarboxylic dianhydride (0.96 g, 3.60 mmol) and 3-picolylamine (1.01 g, 9.35 mmol) were refluxed in *N*,*N*′-dimethylformamide (40 mL) at 100 °C under ambient atmosphere for 6 hours. After cooling, the mixture was subjected to suction filtration and washed several times with methanol, resulting in a yellow-green precipitate (1.34 g, yield: 83%). The formation of 3-picoNDI was confirmed by ^{1}H-NMR spectroscopy.

1w. 3pmNDI (0.13 g, 0.28 mmol) and tin(II) chloride dihydrate (0.057 g, 0.30 mmol) were left to stand in 12 M HCl (40 mL), resulting in the formation of pale yellow crystals within

one week (yield: 54%, 0.13 g). Calcd for [H_2**3pmNDI**][$SnCl_6$]·H_2O = $C_{26}H_{20}Cl_6N_4O_5Sn$, C, 39.04; H, 2.52; N, 7.00. Found C, 38.66; H, 2.44; N, 6.82%.

1. 3pmNDI (0.1238 g, 0.28 mmol) and tin(II) chloride dihydrate (0.0574 g, 0.25 mmol) were refluxed in 12 M HCl (30 mL) at 100 °C for 6 hours, producing reddish-brown crystals (0.1334 g, yield: 68%). Calcd for [$H_2$3pmNDI][$SnCl_6$] = $C_{26}H_{18}Cl_6N_4O_4Sn$, C, 39.94; H, 2.32; N, 7.17. Found C, 39.96; H, 2.18; N, 6.99%.

Physical measurements

Single-crystal X-ray diffraction data were collected using an XtaLAB Synergy instrument. The structures were determined through direct methods with SHELXT[44] and refined using the SHELXL program, employing full-matrix least-squares refinement.[45] Hydrogen atoms were refined geometrically with a riding model. Detailed crystallographic data are summarized in Table S1 (ESI†). Elemental analyses were conducted using an Elementar Vario Micro Cube analyzer. PXRD data were obtained on a RIGAKU RINT-Ultima III X-ray diffractometer (40 kV/40 mA) using Cu Kα radiation (λ = 1.5406 Å) across a 2θ range of 2–30°, with a step width of 1.0°. ESR spectra were recorded using a JEOL JES-RE3X paramagnetic spectrometer. Diffuse reflectance spectra were measured with a JASCO V-670 UV/Vis spectrophotometer, which is equipped with an integrating sphere unit ISN-723. The luminescence spectrum of the powder sample was recorded on a SHIMADZU RF-5300PC spectrofluorophotometer. DC electrical measurements were conducted on unmodified powder samples. Approximately 50 mg of the powders were pressed using a standard 5 mm die at 150 kgf cm^{-2} for 3 min and placed between two gold-coated stainless steel electrodes. Data were collected using a BioLogic VMP3 multichannel potentiostat/galvanostat (Science Instruments) over a voltage range of −2 to 2 V with a scan rate of 20 mV s^{-1}. Three-point bending tests were performed using a SHIMADZU EZ-SX Table-top Universal Testing Instrument. Nanoindentation tests were conducted with a Bruker Hysitron TI Premier Nanomechanical Test Instrument equipped with a diamond Berkovich tip. During these measurements, the crystal faces were indented using a load-controlled mode consisting of a 5-second loading phase, a 2-second holding phase, and a 5-second unloading phase. Photothermal conversion data were recorded using a Testo-871.

Computational methods

DFT calculations in this study were performed using the Vienna *Ab initio* Simulation Package (VASP).[46] The generalized gradient approximation with the Perdew–Burke–Ernzerhof functional was employed.[47] Dispersion corrections were applied using Grimme's D3 scheme with Becke–Johnson damping.[48] The projector augmented wave method[49] was used for the pseudopotential. For Brillouin-zone integration, only Γ point was considered. A plane-wave cutoff energy of 500 eV was applied. The convergence criterion for the electronic self-consistent field loop was set to 1.0 × 10^{-5} eV. Atomic positions and lattice constants were optimized until the forces on all atoms were below 0.03 eV $Å^{-1}$. The wavefunctions were extracted from the DFT calculation results using VASPKIT[50] and visualized with VESTA.[51]

Author contributions

S. K. and Y. K. (Y. Koide) supervised the study. S. M. conducted the experimental work and data analysis. R. S. and M. T. performed the nanoindentation experiments. M. S. and M. K. carried out the photothermal conversion measurements. N. O. and S. U. conducted electronic conductivity measurements. T. F., M. O. and S. H. collected the diffuse reflectance spectroscopic data. Y. T. performed the theoretical calculations. Y. K. (Y. Kim) contributed to scientific discussions. All authors were involved in writing the manuscript.

Data availability

All relevant data have been included in the paper and ESI.†

Conflicts of interest

There are no conflicts to declare.

Acknowledgements

This work was supported by KAKENHI Grant Number JP22K14698. This work was also supported by the Grant-in-Aid for Transformative Research Areas (A) ''Supra-ceramics'' (JSPS KAKENHI Grant Number JP23H04636, JP23H04614, JP 23H04617, JP23H04613 and JP22H05146). The computations in this work were performed using the computer facilities at the Research Institute for Information Technology, Kyushu University, at the Supercomputer Center, the Institute for Solid State Physics, the University of Tokyo, and at Cyberscience Center, Tohoku University.

References

1 (*a*) E. Li, K. Jie, F. Huang, M. Liu, X. Sheng, W. Zhu and F. Huang, *Chem. Soc. Rev.*, 2020, **49**, 1517–1544; (*b*) T. Ogoshi, Y. Shimada, Y. Sakata, S. Akine and T. Yamagishi, *J. Am. Chem. Soc.*, 2017, **139**, 5664–5667; (*c*) K. Ohno, Y. Kusano, S. Kaizaki, A. Nagasawa and T. Fujihara, *Inorg. Chem.*, 2018, **57**, 14159–14169.

2 (*a*) S. Perruchas, X. F. Le Goff, S. Maron, I. Maurin, F. Guillen, A. Garcia, T. Gacoin and J.-P. Boilot, *J. Am. Chem. Soc.*, 2010, **132**, 10967–10969; (*b*) M. Krikorian, S. Liu and T. M. Swager, *J. Am. Chem. Soc.*, 2014, **136**, 2952–2955; (*c*) N. M.-W. Wu, M. Ng and V. W.-W. Yam, *Angew. Chem., Int. Ed.*, 2019, **58**, 3027–3031; (*d*) T. Seki, K. Ida and H. Ito, *Mater. Chem. Front.*, 2018, **2**, 1195–1200.

3 (*a*) S. Kusumoto, Y. Kim and S. Hayami, *Coord. Chem. Rev.*, 2023, **475**, 214890; (*b*) S. Kusumoto, R. Suzuki, M. Tachibana, Y. Sekine, Y. Kim and S. Hayami, *Chem. Commun.*, 2022, **58**, 5411–5414; (*c*) P. Naumov, S. Chizhik, M. K. Panda, N. K. Nath and

E. Boldyreva, *Chem. Rev.*, 2015, **115**, 12440–12490; (*d*) M. K. Panda, S. Ghosh, N. Yasuda, T. Moriwaki, G. D. Mukherjee, C. M. Reddy and P. Naumov, *Nat. Chem.*, 2015, **7**, 65–72; (*e*) P. Naumov, D. P. Karothu, E. Ahmed, L. Catalano, P. Commins, J. M. Halabi, M. B. Al-Handawi and L. Li, *J. Am. Chem. Soc.*, 2020, **142**, 13256–13272; (*f*) E. Ahmed, D. P. Karothu and P. Naumov, *Angew. Chem., Int. Ed.*, 2018, **57**, 8837–8846; (*g*) W. M. Awad, D. W. Davies, D. Kitagawa, J. Mahmoud Halabi, M. B. Al-Handawi, I. Tahir, F. Tong, G. CampilloAlvarado, A. G. Shtukenberg, T. Alkhidir, Y. Hagiwara, M. Almehairbi, L. Lan, S. Hasebe, D. P. Karothu, S. Mohamed, H. Koshima, S. Kobatake, Y. Diao, R. Chandrasekar, H. Zhang, C. C. Sun, C. Bardeen, R. O. Al-Kaysi, B. Kahr and P. Naumov, *Chem. Soc. Rev.*, 2023, **52**, 3098–3169.

4 M. Kato, H. Ito, M. Hasegawa and K. Ishii, *Chem. – Eur. J.*, 2019, **25**, 5105–5112.

5 (*a*) T. Fu, Y.-L. Wei, C. Zhang, L.-K. Li, X.-F. Liu, H.-Y. Li and S.-Q. Zang, *Chem. Commun.*, 2020, **56**, 13093–13096; (*b*) M. Ikeya, G. Katada and S. Ito, *Chem. Commun.*, 2019, **55**, 12296–12299; (*c*) S.-J. Yoon, J. W. Chung, J. Gierschner, K. S. Kim, M.-G. Choi, D. Kim and S. Y. Park, *J. Am. Chem. Soc.*, 2010, **132**, 13675–13683.

6 (*a*) M. B. Al-Handawi, P. Commins, A. S. Dalaq, P. A. Santos-Florez, S. Polavaram, P. Didier, D. P. Karothu, Q. Zhu, M. Daqaq, L. Li and P. Naumov, *Nat. Commun.*, 2024, **15**, 8095; (*b*) S. Dai, J. Zhong, X. Yang, C. Chen, L. Zhou, X. Liu, J. Sun, K. Ye, H. Zhang, L. Li, P. Naumov and R. Lu, *Angew. Chem., Int. Ed.*, 2024, **63**, e202320223; (*c*) P. Gupta, D. P. Karothu, E. Ahmed, P. Naumov and N. K. Nath, *Angew. Chem., Int. Ed.*, 2018, **57**, 8498–8502; (*d*) M. Annadhasan, D. Prasad Karothu, R. Chinnasamy, L. Catalano, E. Ahmed, S. Ghosh, P. Naumov and R. Chandrasekar, *Angew. Chem., Int. Ed.*, 2020, **59**, 13821–13830; (*e*) P. Commins, M. B. Al-Handawi, D. P. Karothu, G. Raj and P. Naumov, *Chem. Sci.*, 2020, **11**, 2606–2613; (*f*) T. Seki, C. Feng, K. Kashiyama, S. Sakamoto, Y. Takasaki, T. Sasaki, S. Takamizawa and H. Ito, *Angew. Chem., Int. Ed.*, 2020, **59**, 8839–8843.

7 (*a*) M. Jin, T. Sumitani, H. Sato, T. Seki and H. Ito, *J. Am. Chem. Soc.*, 2018, **140**, 2875–2879; (*b*) M. Yoshida and M. Kato, *Coord. Chem. Rev.*, 2018, **355**, 101–115; (*c*) H. Ito, T. Saito, N. Oshima, N. Kitamura, S. Ishizaka, Y. Hinatsu, M. Wakeshima, M. Kato, K. Tsuge and M. Sawamura, *J. Am. Chem. Soc.*, 2008, **130**, 10044–10045.

8 (*a*) S. Kusumoto, K. Inaba, H. Suda, M. Nakaya, R. Tokunaga, P. Thuery, R. Haruki, T. Kanazawa, S. Nozawa, Y. Kim, S. Hayami and Y. Koide, *Inorg. Chem.*, 2023, **39**, 16222–16227; (*b*) P. Kar, M. Yoshida, Y. Shigeta, A. Usui, A. Kobayashi, T. Minamidate, N. Matsunaga and M. Kato, *Angew. Chem., Int. Ed.*, 2017, **56**, 2345–2349; (*c*) K. M. Fgrpaß, L. M. Peschel, J. A. Schachner, S. M. Borisov, H. Krenn, F. Belaj and N. C. Mösch-Zanetti, *Angew. Chem., Int. Ed.*, 2021, **60**, 13401–13404; (*d*) S. Xue, G. F. B. Solre, X. Wang, L. Wang and Y. Guo, *Chem. Commun.*, 2022, **58**, 1954–1957; (*e*) Y. Zhao, L. Wang, S. Xue and Y. Guo, *Inorg. Chem. Front.*, 2022, **9**, 4127–4135.

9 (*a*) K. Imaoka, H. S. Kim, Y. Yamamoto, S. Fukutomi, L.-M. Chamoreau, L. Qu, H. Iguchi, Y. Tsuchiya, T. Ono, F. Mathevet and C. Adachi, *Adv. Funct. Mater.*, 2024, **34**, 2409299; (*b*) L. Qu, H. Iguchi, S. Takaishi, F. Habib, C. F. Leong, D. M. D'Alessandro, T. Yoshida, H. Abe, E. Nishibori and M. Yamashita, *J. Am. Chem. Soc.*, 2019, **141**, 6802–6806; (*c*) B. Dutta, A. Dey, C. Sinha, P. P. Ray and M. H. Mir, *Inorg. Chem.*, 2019, **58**, 5419–5422; (*d*) H. Kyu Lee, Y. Oruganti, J. Lee, S. Han, J. Kim, D. Moon, M. Kim, D.-W. Lim and H. R. Moon, *J. Mater. Chem. A*, 2024, **12**, 795–801.

10 (*a*) R. Paolesse, S. Nardis, D. Monti, M. Stefanelli and C. D. Natale, *Chem. Rev.*, 2017, **117**, 2517–2583; (*b*) V. Schroeder, S. Savagatrup, M. He, S. Lin and T. M. Swager, *Chem. Rev.*, 2019, **119**, 599–663.

11 (*a*) L. Li, D. P. Karothu, P. Commins, M. B. Al-Handawi, J. M. Halabi, S. Schramm, J. Weston, R. Rezgui and P. Naumov, *Chem. Sci.*, 2019, **10**, 7327–7332; (*b*) F. Terao, M. Morimoto and M. Irie, *Angew. Chem., Int. Ed.*, 2012, **51**, 901–904; (*c*) S. Kusumoto, K. Wakabayashi, K. Rakumitsu, J. Harrowfield, Y. Kim and Y. Koide, *Chem. – Eur. J.*, 2024, e202401564; (*d*) S. Kobatake, S. Takami, H. Muto, T. Ishikawa and M. Irie, *Nature*, 2007, **446**, 778–781; (*e*) L. Lan, L. Li, Q. Di, X. Yang, X. Liu, P. Naumov and H. Zhang, *Adv. Mater.*, 2022, **34**, 2200471; (*f*) S. C. Sahoo, M. K. Panda, N. K. Nath and P. Naumov, *J. Am. Chem. Soc.*, 2013, **135**, 12241–12251.

12 (*a*) P. Marandi, D. Saini, K. Arora, R. Garg, U. Sarkar, K. Parida, D. Mandal and P. P. Neelakandan, *J. Am. Chem. Soc.*, 2024, **146**, 26178–26186; (*b*) B. Sun, Y.-Z. Long, Z.-J. Chen, S.-L. Liu, H.-D. Zhang, J.-C. Zhang and W.-P. Han, *J. Mater. Chem. C*, 2014, **2**, 1209–1219; (*c*) Y. Zang, D. Huang, C.-A. Di and D. Zhu, *Adv. Mater.*, 2016, **28**, 4549–4555.

13 (*a*) A. K. Geim and I. V. Grigorieva, *Nature*, 2013, **499**, 419–425; (*b*) P. A. Kollman, *Chem. Rev.*, 1977, **10**, 365–371.

14 (*a*) F. J. M. Hoeben, P. Jonkheijm, E. W. Meijer and A. P. H. J. Schenning, *Chem. Rev.*, 2005, **105**, 1491–1546; (*b*) J. Shen, Y. Zhu, X. Yang and C. Li, *Chem. Commun.*, 2012, **48**, 3686–3699; (*c*) J. Cornil, D. Beljonne, J.-P. Calbert and J.-L. Brédas, *Adv. Mater.*, 2001, **13**, 1053–1067.

15 (*a*) S. Kusumoto, A. Sugimoto, Y. Zhang, Y. Kim, M. Nakamura, L. F. Lindoy and S. Hayami, *Inorg. Chem.*, 2021, **60**, 1294–1298; (*b*) Y. Sekine, S. Kusumoto, A. Sugimoto, M. Nakaya and S. Hayami, *Cryst. Growth Des.*, 2023, **23**, 2013–2017; (*c*) S. Hayashi, F. Ishiwari, T. Fukushima, S. Mikage, Y. Imamura, M. Tashiro and M. Katouda, *Angew. Chem., Int. Ed.*, 2020, **59**, 16195–16201; (*d*) A. J. Thompson, J. R. Price, A. I. C. Orué, J. McMurtrie, A. J. Nair and J. K. Clegg, *Chem. Soc. Rev.*, 2021, **50**, 11725–11740; (*e*) T. Matsuo, J. Kuwabara, T. Kanbara and S. Hayashi, *J. Phys. Chem. Lett.*, 2023, **14**, 6577–6582; (*f*) A. Worthy, A. Grosjean, M. C. Pfrunder, Y. Xu, C. Yan, G. Edwards, J. K. Clegg and J. C. McMurtrie, *Nat. Chem.*, 2018, **10**, 65–69; (*g*) D. P. Karothu, G. Dushaq, E. Ahmed, L. Catalano, M. Rasras and P. Naumov, *Angew. Chem., Int. Ed.*, 2021, **60**, 26151–26157.

16 (*a*) L. Pejov, M. K. Panda, T. Moriwaki and P. Naumov, *J. Am. Chem. Soc.*, 2017, **139**, 2318–2328; (*b*) P. Commins, D. P. Karothu and P. Naumov, *Angew. Chem., Int. Ed.*, 2019, **58**, 10052–10060.

17 (*a*) E. P. Kenny, A. C. Jacko and B. J. Powell, *Angew. Chem., Int. Ed.*, 2019, **58**, 15082–15088; (*b*) W. Wu, K. Chen, T. Wang, N. Wang, X. Huang, L. Zhou, Z. Wang and H. Hao, *J. Mater. Chem. C*, 2023, **11**, 2026–2052; (*c*) T. Seki, N. Hoshino, Y. Suzuki and S. Hayashi, *CrystEngComm*, 2021, **23**, 5686–5696.

18 (*a*) C. Zhou, H. Lin, S. Lee, M. Chaaban and B. Ma, *Mater. Res. Lett.*, 2018, **6**, 552–569; (*b*) Y. Dong, Y. Han, R. Chen, Y. Lin and B.-B. Cui, *J. Lumin.*, 2022, **249**, 119013.

19 J. Hermann, R. A. DiStasioJr and A. Tkatchenko, *Chem. Rev.*, 2017, **117**, 4714–4758.

20 (*a*) K. Maeda, T. Motohashi, R. Ohtani, K. Sugimoto, Y. Tsuji, A. Kuwabara and S. Horike, *Sci. Technol. Adv. Mater.*, 2024, **25**, 1; (*b*) A. Kojima, K. Teshima, Y. Shirai and T. Miyasaka, *J. Am. Chem. Soc.*, 2009, **131**, 6050–6051; (*c*) M. M. Lee, J. Teuscher, T. Miyasaka, N. M. Takurou and H. J. Snaith, *Science*, 2012, **338**, 643–647.

21 G. Xing, N. Mathews, S. S. Lim, N. Yantara, X. Liu, D. Sabba, M. Grätzel, S. Mhaisalkar and T. C. Sum, *Nat. Mater.*, 2014, **13**, 476–480.

22 (*a*) S. D. Stranks and H. J. Snaith, *Nat. Nanotechnol.*, 2015, **10**, 391–402; (*b*) K. Lin, J. Xing, L. N. Quan, F. P. G. D. Arquer, X. Gong, J. Lu, L. Xie, W. Zhao, D. Zhang, C. Yan, W. Li, X. Liu, Y. Lu, J. Kirman, E. H. Sargent, Q. Xiong and Z. Wei, *Nature*, 2018, **562**, 245–248.

23 Y. Wang and S. Pan, *Coord. Chem. Rev.*, 2016, **323**, 15–35.

24 (*a*) S. Sun, F. H. Isikgor, Z. Deng, F. Wei, G. Kieslich, P. D. Bristowe, J. Ouyang and A. K. Cheetham, *ChemSusChem*, 2017, **10**, 3740–3745; (*b*) W. Wei, H. Gao, X. Lei, G. Feng and W. Li, *Inorg. Chem. Commun.*, 2017, **85**, 45–48; (*c*) S. Sun, Y. Fang, G. Kieslich, T. J. White and A. K. Cheetham, *J. Mater. Chem. A*, 2015, **3**, 18450–18455; (*d*) Q. Tu, I. Spanopoulos, E. S. Vasileiadou, X. Li, M. G. Kanatzidis, G. S. Shekhawat and V. P. Dravid, *ACS Appl. Mater. Interfaces*, 2020, **12**, 20440–20447.

25 (*a*) X. Guo, F. S. Kim, M. J. Seger, S. A. Jenekhe and M. D. Watson, *Chem. Mater.*, 2012, **24**, 1434–1442; (*b*) B. A. Johnson, A. Bhunia, H. Fei, S. M. Cohen and S. Ott, *J. Am. Chem. Soc.*, 2018, **140**, 2985–2994.

26 (*a*) B. A. Jones, A. Facchetti, M. R. Wasielewski and T. J. Marks, *J. Am. Chem. Soc.*, 2007, **129**, 15259–15278; (*b*) B. A. Jones, A. Facchetti, T. J. Marks and M. R. Wasielewski, *Chem. Mater.*, 2007, **19**, 2703–2705.

27 (*a*) Y. Kumar, S. Kumar, K. Mandal and P. Mukhopadhyay, *Angew. Chem., Int. Ed.*, 2018, **57**, 16318–16322; (*b*) R. P. Ortiz, H. Herrera, C. Seoane, J. L. Segura, A. Facchetti and T. J. Marks, *Chem. – Eur. J.*, 2012, **18**, 532–543.

28 (*a*) S. Guha and S. Saha, *J. Am. Chem. Soc.*, 2010, **132**, 17674–17677; (*b*) T. Ono, Y. Tsukiyama, S. Hatanaka, Y. Sakatsume, T. Ogoshi and Y. Hisaeda, *J. Mater. Chem. C*, 2019, **7**, 9726–9734.

29 (*a*) Z. Chen, Y. Zheng, H. Yan and A. Facchetti, *J. Am. Chem. Soc.*, 2009, **131**, 8–9; (*b*) Y. Wu, S. Schneider, C. Walter, A. Haider Chowdhury, B. Bahrami, H.-C. Wu, Q. Qiao, M. F. Toney and Z. Bao, *J. Am. Chem. Soc.*, 2020, **142**, 392–406.

30 (*a*) S. Kumar and P. Mukhopadhyay, *Green Chem.*, 2018, **20**, 4620–4628; (*b*) S. Kumar, M. R. Ajayakumar, G. Hundal and P. Mukhopadhyay, *J. Am. Chem. Soc.*, 2014, **136**, 12004–12010; (*c*) S. Saha, *Acc. Chem. Res.*, 2018, **51**, 2225–2236.

31 B. Lü, Y. Chen, P. Li, B. Wang, K. Müllen and M. Yin, *Nat. Commun.*, 2019, **10**, 767.

32 (*a*) M. Đaković, M. Borovina, M. Pisačić, C. B. Aakerçy, Ž. Soldin, B.-M. Kukovec and I. Kodrin, *Angew. Chem., Int. Ed.*, 2018, **57**, 14801–14805; (*b*) M. Pisačić, I. Kodrin, I. Biljan and M. Đaković, *CrystEngComm*, 2021, **23**, 7072–7080; (*c*) M. Pisačić, I. Kodrin, A. Trninić and M. Đaković, *Chem. Mater.*, 2022, **34**, 2439–2448.

33 (*a*) S. Hayashi and T. Koizumi, *Angew. Chem., Int. Ed.*, 2016, **55**, 2701–2704; (*b*) M. Annadhasan, A. R. Agrawal, S. Bhunia, V. V. Pradeep, S. S. Zade, C. M. Reddy and R. Chandrasekar, *Angew. Chem., Int. Ed.*, 2020, **59**, 13852–13858; (*c*) S. Hayashi and T. Koizumi, *Chem.–Eur. J.*, 2018, **24**, 8507–8512; (*d*) S. Ghosh and M. K. Mishra, *Cryst. Growth Des.*, 2021, **21**, 2566–2580.

34 (*a*) P. Lasitha, *ChemistrySelect*, 2021, **6**, 7936–7943; (*b*) M. Licchelli, L. Linati, O. A. Biroli, E. Perani, A. Poggi and D. Sacchi, *Chem. – Eur. J.*, 2002, **8**, 5161–5169.

35 S. Liu, X. Pan and H. Liu, *Angew. Chem., Int. Ed.*, 2020, **59**, 5890–5900.

36 X. Li, E.-Y. Park, Y. Kang, N. Kwon, M. Yang, S. Lee, W. J. Kim, C. Kim and J. Yoon, *Angew. Chem., Int. Ed.*, 2020, **59**, 8630–8634.

37 X. Lu, L. Sun, P. Jiang and X. Bao, *Adv. Mater.*, 2019, **31**, 1902044.

38 S. Wang, S. Li, J. Xiong, Z. Lin, W. Wei and Y. Xu, *Chem. Commun.*, 2020, **56**, 7399–7402.

39 M.-Q. Li, M. Zhao, L.-Y. Bi, Y.-Q. Hu, G. Gou, J. Li and Y.-Z. Zheng, *Inorg. Chem.*, 2019, **58**, 6601–6608.

40 C. M. Hessel, V. P. Pattani, M. Rasch, M. G. Panthani, B. Koo, J. W. Tunnell and B. A. Korgel, *Nano Lett.*, 2011, **11**, 2560–2566.

41 D. Wang, X. Kan, C. Wu, Y. Gong, G. Guo, T. Liang, L. Wang, Z. Li and Y. Zhao, *Chem. Commun.*, 2020, **56**, 5223–5226.

42 S. Kusumoto, T. Mio, K. Rakumitsu, M. Shimabukuro, M. Kobayashi, T. Fukui, N. Hamamoto, T. Ishizaki, Y. Kim and Y. Koide, *J. Mater. Chem. C*, 2025, **13**, 3408–3413.

43 S. Masuda, S. Kusumoto, M. Okamura, S. Hikichi, R. Tokunaga, S. Hayami, Y. Kim and Y. Koide, *Dalton Trans.*, 2023, **52**, 10531–10536.

44 G. M. Sheldrick, *Acta Crystallogr., Sect. A*, 2015, **71**, 3–8.

45 G. M. Sheldrick, *Acta Crystallogr., Sect. C:Cryst. Struct. Commun.*, 2015, **71**, 3–8.

46 (*a*) G. Kresse and J. Furthmüller, *Comput. Mater. Sci.*, 1996, **6**, 15–50; (*b*) G. Kresse and D. Joubert, *Phys. Rev. B: Condens. Matter Mater. Phys.*, 1999, **59**, 1758; (*c*) G. Kresse and J. Furthmüller, *Phys. Rev. B: Condens. Matter Mater. Phys.*, 1996, **54**, 11169.

47 J. P. Perdew, K. Burke and M. Ernzerhof, *Phys. Rev. Lett.*, 1996, **77**, 3865–3868.

48 S. Grimme, S. Ehrlich and L. Goerigk, *J. Comput. Chem.*, 2011, **32**, 1456–1465.

49 P. E. Blöchl, *Phys. Rev. B: Condens. Matter Mater. Phys.*, 1994, **50**, 17953–17979.

50 V. Wang, N. Xu, J.-C. Liu, G. Tang and W.-T. Geng, *Comput. Phys. Commun.*, 2021, **267**, 108033.

51 K. Momma and F. Izumi, *J. Appl. Crystallogr.*, 2011, **44**, 1272–1276.

